High-temperature internal friction and dislocations in ice Ih

J. Tatibouet, J. Perez, R. Vassoille

Classification
Physics Abstracts
61.70L

High-temperature internal friction and dislocations in ice I_h

J. Tatibouet, J. Perez and R. Vassoille

Groupe d'Etudes de Métallurgie Physique et de Physique des Matériaux, UA 341, INSA de Lyon, Bât. 502, 69621 Villeurbanne Cedex, France

(*Reçu le 9 mai 1985, accepté le 4 septembre 1985*)

Résumé. — Des mesures de frottement interne à très basses fréquences (10^{-3}-1 Hz) ont été effectuées à haute température ($T > 230$ K) sur de la glace monocristalline. Ces expériences ont été complétées par des essais de microfluage. Les résultats expérimentaux montrent qu'il est nécessaire de tenir compte de l'ensemble du réseau de dislocation. Un modèle est proposé en faisant l'hypothèse de l'interaction entre les dislocations glissant dans le plan de base et la montée de segments de dislocations dans les plans non basaux. La simulation numérique appliquée à la fois au frottement interne et au microfluage rend compte des résultats expérimentaux.

Abstract. — High temperature internal friction measurements at very low frequencies (10^{-3}-1 Hz) have been done on single crystals of ice. Experiments were completed by microcreep experiments. These experiments show that it is necessary to take into account the whole network of dislocation. A model is proposed on the assumption that the dislocation glide in the basal plane interacts with the climb of dislocation segments in the non-basal plane. Simulations of both internal friction and microcreep are in agreement with experimental results.

1. Introduction.

In order to understand the internal friction measurements made at high temperatures it is desirable to recall some specific properties concerning the movement of dislocations in ice.

Ice I_h is a crystalline solid only from the point of view of oxygen atoms (würtzite type). Hydrogen atoms are disordered and water molecules in the structure have to obey the Bernal and Fowler rules (i.e. the water molecule is conserved in the structure and only one hydrogen atom has to be between two oxygen atoms). Non-respect of these rules introduces defects such as ionic defects (OH^-, H_3O^+) and L or D rotational (or bjerrum) defects. Due to the proton disorder the movement of a dislocation through the ice crystal cannot be so simple as in usual crystals.

Thus, it has been proposed by Glen [1] that the disorder of the protons presents a major obstacle to the glide of dislocation because water molecules behind a moving dislocation may not be correctly oriented to form normal hydrogen bonds. On this assumption, different models were developed [2-5], but they cannot explain why dislocation velocity becomes non-linear with stress as the temperature rises [6].

A new attempt was made by Perez *et al.* [7, 8] which proposed a non-crystalline core structure for dislocations in ice especially in the high-temperature range ($T > 240$ K).

The precise mechanisms for dislocation motion are not yet well described by either model in the case of real crystals. The aim of the present work is to bring about more experimental features to solve this problem. Mechanical damping measurements and more generally the study of microplasticity, are well suited to this purpose as high temperature internal friction is clearly attributed to dislocation motion [9].

Previous papers concerning high-temperature internal friction [10] did not take into account some parameters, particularly the dependence of the internal friction on deformation amplitude. Thus, a more global analysis of internal friction results is done in order to make a closer comparison between internal friction and microplasticity measurements.

2. Experimental procedure.

Experiments were performed by using an inverted torsional apparatus developed in the laboratory [11]. A torque is transmitted to the specimen ($8 \times 2 \times 50$ mm^3) by the interaction between a small permanent magnet and a magnetic field produced by Helmholtz coils. For small strain, the intensity of the current in the coils is proportional to the stress. Strain is detected by

an optical method using differential photovoltaïc cells. Strain and stress signals are both sent to a calculator through a memory. Either stress or strain can be imposed so that creep, or stress relaxation and internal friction experiments can be performed with the same apparatus. Sinusoïdal stress or strain leads to internal friction (tan. φ) and to a parameter proportional to the shear modulus. The frequency of the stress or strain is in the range 10^{-4}-1 Hz. A liquid nitrogen cryostat permitted measurements from 80 to 273 K. Plastic deformation (up to 3 %) by creep in torsion is also possible *in situ*.

By applying a step of current in the coils, microcreep experiments were performed for different values of stress and for temperatures varying from 210 to 272 K. Stress is applied to the specimen for a short time (20 s) and removed for a long time (10 min) before applying stress again. Microcreep experiments have also been performed during longer loading time ($t = 10^3$ s corresponding to our 10^{-3} Hz internal friction measurements). Figure 1 shows such curves thus obtained.

We have also noted that the dislocation density remains constant during experiments by making two runs of measurements on each specimen and obtaining the same value for strain-rate in all cases. Due to the difficulty of determining the strain rate at the initial moment, $\dot{\varepsilon}$ was measured at $t = 20$ s.

Specimens are mechanically cut from single-crystals grown by the Bridgman method in « the Laboratoire de Glaciologie » (Grenoble). Their orientation was determined by X-ray Laüe diagram. Some of the specimens were HF-doped by diffusion.

3. Experimental results.

Figure 2a shows high-temperature internal friction measured at different frequencies for a freshly grown non-deformed single crystal. The internal friction increases rapidly when the frequency is decreased and at constant frequency the internal friction is very temperature-dependent. Figure 2b shows the strain rate *vs.* stress from microcreep experiments performed on the same specimen up to 270 K. $\dot{\varepsilon}$ becomes non-linear with stress when temperature is higher than 256 K.

After plastic deformation of the specimen made, *in situ* ($\varepsilon_p = 1.8$ %) we obtain results shown in figure 2 : figure 2a shows internal friction *vs.* temperature.

A very important increase of internal friction can be noticed when the temperature increases. On figure 2b we have plotted results from microcreep measurements made on the same plastically deformed specimen. The

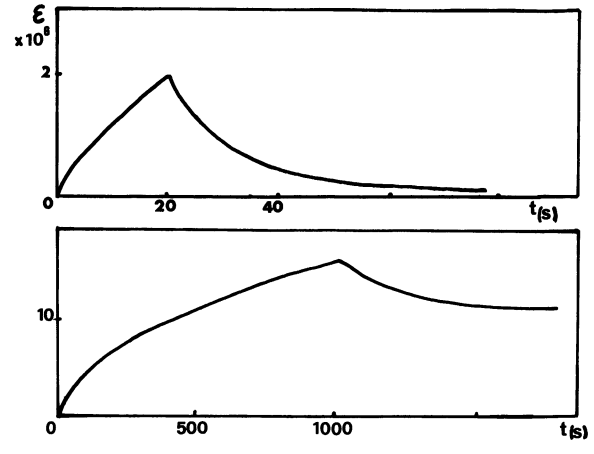

Fig. 1. — Typical microcreep curves obtained on single crystals for different loading times. $T = 262$ K; $\sigma = 10^5$ N m^{-2} (Elastic part is removed).

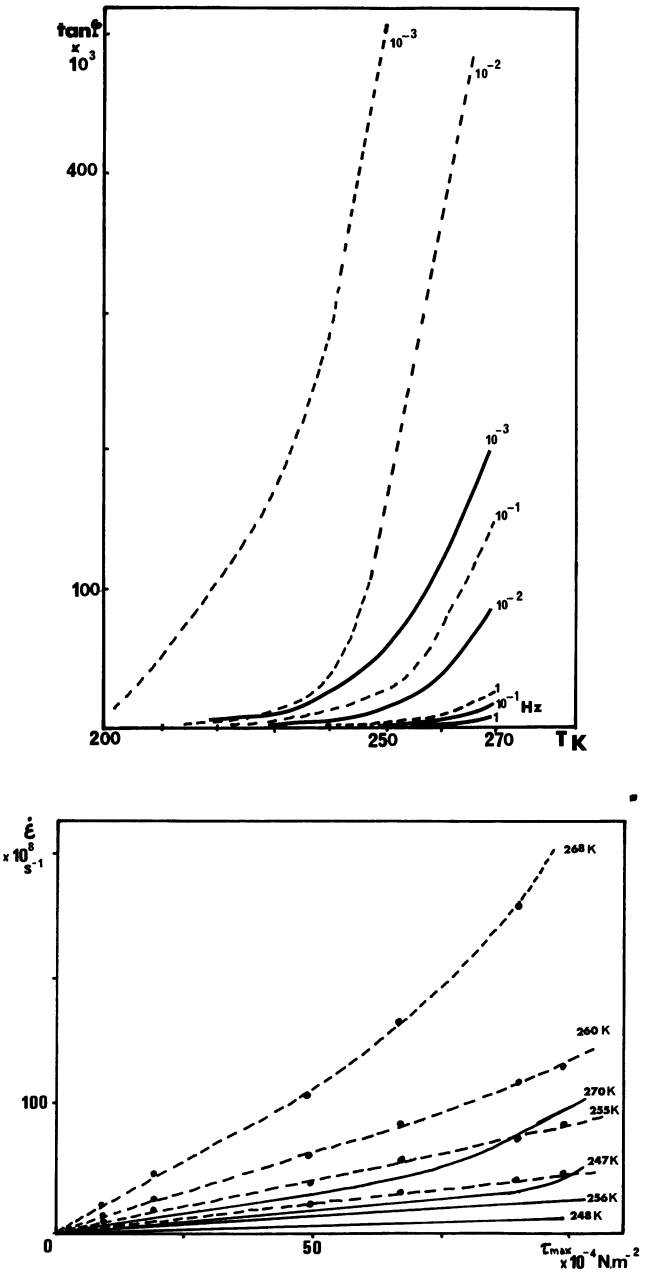

Fig. 2. — a) Internal friction *versus* temperature; $\varepsilon_{max} = 2 \times 10^{-5}$. b) Strain-rate *versus* stress. (Non deformed single crystal ; continuous lines. Plastically deformed single crystal ($\varepsilon_p = 1.8$ %)-dashed lines.)

strain rate $\dot{\varepsilon}$ is increased by a factor 3.5 to 4 after plastic deformation.

We have also performed the same experiments on HF-doped specimen (HF concentration estimated from relaxation peak temperature $\simeq$ 40 ppm) and results are shown in figures 3a and 3b. In this case, the rise in internal friction appears at temperatures lower than in pure ice (below 200 K) and the strain rate is increased and becomes non-linear for temperature as low as 240 K. As the high-temperature internal friction of ice is known to be amplitude dependent [9] all the internal friction measurements were done at constant maximum amplitude ($\varepsilon_{max} = 5 \times 10^{-5}$). The experiments were apparently performed at constant structure, because we have verified that after every measurement at 10^{-2} and 10^{-3} Hz we found exactly the same initial internal friction as that obtained at 1 Hz.

Of course, the amplitude dependence of internal friction has also been studied. Experiments were performed at different frequencies with the maximum amplitude varying from $\varepsilon_{max} = 2 \times 10^{-5}$ to 7.5×10^{-5}, corresponding to maximum stress σ_{max} from 1.5×10^5 to 6×10^5 N.m^{-2}. Figure 4 shows internal friction *vs.* maximum stress for pure ice (t//C) at 251, 260, 265, and 270 K. The variation becomes important when temperature is increased but even at 251 K for the lower frequencies (10^{-2}-10^{-3} Hz) we can notice a dependence on stress. Dependence on maximum amplitude remains weak for 1 Hz measurements for $\varepsilon_{max} < 10^{-4}$ and temperature below 265 K in agreement with results obtained by Vassoille [9].

4. Discussion.

As we have seen before, high-temperature internal friction exhibits a strong dependence on the strain amplitude. So, before going forward with a more complete analysis, it is necessary to correct our experimental values in order to obtain local values of internal friction, because the shape of the specimen and the torsional mode for deformation induce an important strain gradient. The problem has been studied by several authors [12, 13] and leads to the expression

$$\tan_l \varphi = \tan_g \varphi \left(1 + \frac{\tau_{max}}{3 \tan_g \varphi} \cdot \frac{\partial \tan_g \varphi}{\partial \tau_{max}} \right)$$

where $\tan_l \varphi$ and $\tan_g \varphi$ are the local and global (measured) values of the internal friction respectively. τ_{max} is the maximum shear stress during measurement which is obtained from the measured strain and modulus; $\partial \tan_g \varphi / \partial \tau_{max}$ is derived from the curves of figure 4 for a deformation taken as $\varepsilon_{max} = 5 \times 10^{-5}$ which is a value well suited to all the measurements. Such corrections lead to an increase in internal friction values for 10^{-2} and 10^{-3} Hz experiments above 250 K and are negligible for higher frequency measurements.

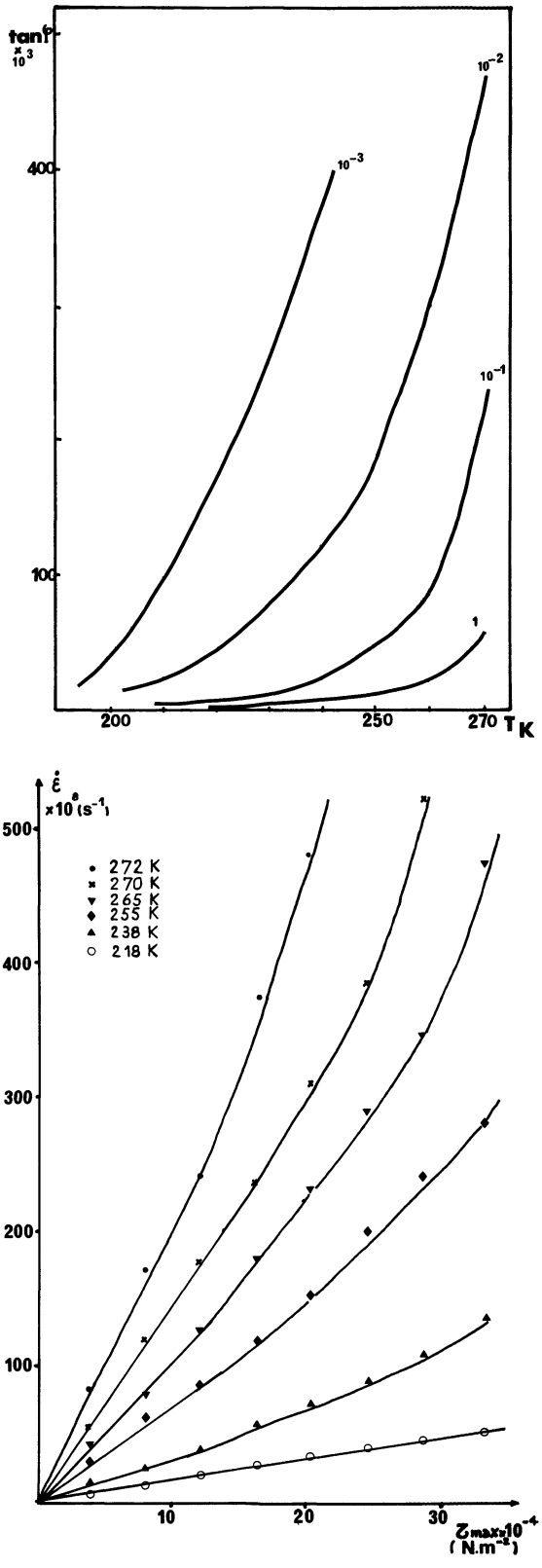

Fig. 3. — a) internal friction *versus* temperature. $\varepsilon_{max} = 2 \times 10^{-5}$. b) Strain-rate *versus* stress. HF-doped single crystal (40 ppm HF).

High temperature internal friction is attributed to dislocation motion induced by the cyclic stress and its values increase as the density of dislocation increases

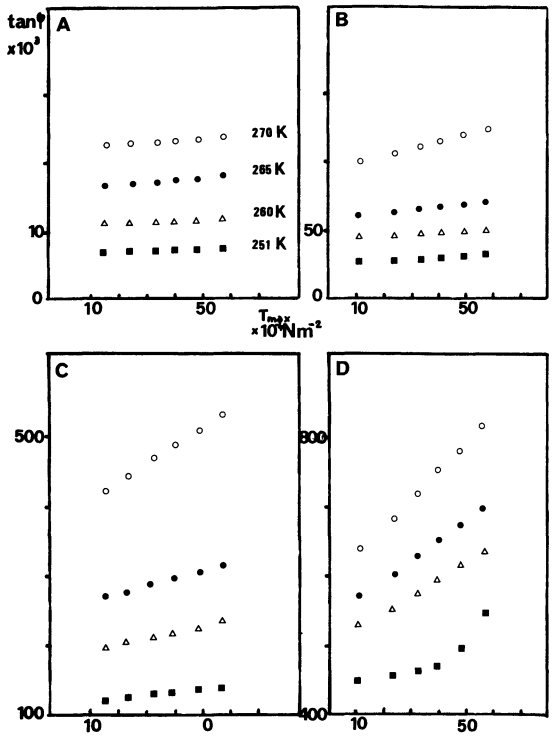

Fig. 4. — Internal friction *versus* maximum stress at different temperatures and frequencies. Non-deformed single crystal. A) 1 Hz B) 10^{-1} Hz C) 10^{-2} Hz D) 10^{-3} Hz.

after a plastic deformation. In the same way, strain rate increases with dislocation density according to Orowan's relation $\dot{\varepsilon} = \alpha . \rho_d v b$ where ρ_d is the density of mobile dislocations. Our microcreep measurements show that a plastic deformation of 1.8 % induces an increase of the dislocation density by a factor 3.5 to 4.

The temperature dependence of the phenomenon is not simple : in figure 5 we have plotted log $\tan_1 \varphi$ *versus* $1/T$ for different frequencies for a plastically deformed specimen. Figure 5 also shows a plot $\dot{\varepsilon}(0)$ *versus* $1/T$ from microcreep experiment performed on the same specimen ($\dot{\varepsilon}(0)$ is the strain rate extrapolated at $\sigma_{max} = 0$). These plots show that different regimes are involved in the dislocation motion.

At lower temperatures (i.e. below 240-235 K) the apparent activation energy of the phenomenon is weater forboth cases : internal friction and microcreep experiments. We obtained a value of 0.23 ± 0.03 eV for pure or HF-doped specimen and a value of 0.32 ± 0.03 eV for aged ice. This activation energy is found to be the same as that of the relaxation peak observed on the specimen at lower temperature (150-180 K) [14]. Although the precise mechanism for the relaxation peak is not fully explained, a rearrangement of water molecules with the help of rotational defects representing deviations from the Bernard and Rowler rules is generally considered to be the physical origin of the phenomenon [15, 16]. That is to say that at lower temperatures (below 240 K) the mechanism

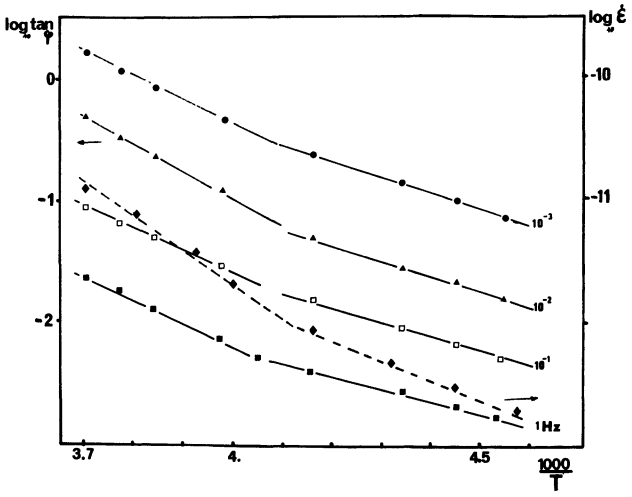

Fig. 5. — a) $\log_{10}$ (internal friction) *versus* inverse of temperature at different frequencies for a deformed specimen. b) $\log_{10}$ (strain-rate) *versus* inverse of temperature for same specimen. ($\dot{\varepsilon}$ is extrapolated at 0)-dashed line.

involved for dislocation motion may be limited by reorientation of water molecules as previously proposed in Glen's hypothesis [1] and further developed by different authors [2-4].

At higher temperatures (above 240 K) the situation seems to be more complex. Higher activation energy can be found with values between 0.30 and 0.55 eV depending on the specimen. In this temperature range we have tried to apply the non-crystalline core model for dislocations [7]. From this model, theoretical values for dislocation velocity and internal friction can be proposed. For low stresses, which is the case in our experiments the internal friction is expressed by :

$$\tan \varphi = \frac{G}{kT} \cdot \frac{1}{v} \cdot \frac{\rho_d b^5}{9 \pi \tau_r}$$

where G = shear modulus, v = frequency of cyclic stress, ρ_d = dislocation density, b = Burgers vector of dislocation and $\tau_r = \tau_0 \exp(2/3)(E/kT)^2$ = mean duration for a movement of an H_2O molecule in the core leading to the glide of the linear defect; E is the difference of energy of a broken hydrogen bond in the core and a hydrogen bond in the vicinity of the non-crystalline core.

Such an expression was well fitted with experiments in the case of the 1 Hz frequency range [8] and would imply that the internal friction is proportional to v^{-1}. Actually, thanks to the frequency scanning experiments previously [10] and here presented, it is possible to show that this is not the case.

In fact in this model it was assumed that the strain rate is time-independent, when the applied stress is constant. For experiments done at 1 Hz [9] for which the cyclic stress is applied during a short time we can consider that this assumption is correct. Of

course, for experiments performed at very low frequencies this is no longer the case as we can notice on microcreep experiments [10]. For internal friction measurements done at 10^{-2} Hz for example correponding to a creep time of 10^2 s the strain rate does decrease, illustrating more complex viscoelastic properties of the material.

The non-proportionality between $\tan\varphi$ and v^{-1} has been previously described using phenomenological expression [10]. Using the formalism developed by Schoek *et al.* [17] :

$$\tan\varphi = C_1\left(\frac{1}{v\tau_r}\right)^n = C_2\left(\frac{\exp\left(-\frac{2}{3}\right)\left(\frac{E}{kT}\right)^2}{v}\right)^n .$$

We found values for n and E which are summarized in table I :

Table I. — *Values of E and n for different types of specimens from plots* a) $\ln\tan\varphi = f(1/T^2)$; V = Const., b) $\ln v = f(1/T^2)$; $\tan\varphi$ = Const., c) $\tan\varphi = f(\ln v)$.

	E(a) eV	$E.\sqrt{n}$(b) eV	n(c)	Corrected E (b) and (c)
Deformed ice $\varepsilon_p = 1.2\ \%$ fresh grown	0.093 ± 0.003	0.070 ± 0.007	0.61	0.095 ± 0.004
Non-deformed ice (aged)	0.094 ± 0.003	0.062 ± 0.004	0.40	0.098 ± 0.007
Deformed ice (aged) $\varepsilon_p = 1.8\ \%$	0.090 ± 0.003	0.08 ± 0.01	0.83	0.092 ± 0.007
HF doped	0.083 ± 0.001	0.056 ± 0.02	0.50	0.079 ± 0.004

Values of E are in good agreement with those determined previously [8] and with theoretical values extrapolated from calculations on interaction of water molecules in ice [18].

For the values of n, a difference can be noticed when specimens are plastically deformed or not, indicating that n may be a distribution parameter on the restoring forces acting on dislocation. This distribution is larger in the case of non-deformed specimens where the dislocation density is weak.

Another important feature is put in evidence when performing microcreep experiments during long loading time (see Fig. 1). In this case, when stress is removed we obtain, for temperatures higher than 250 K, both recovery strain and permanent strain. It indicates that two types of behaviour occurred for dislocation motion. One, which is put in evidence in short time experiments shows a reversible motion for dislocation inducing anelasticity only. The other, which becomes important with long-time experiments is more complex showing that viscoplasticity is added to the anelasticity previously observed.

So, internal friction and microcreep measurements have to be interpreted not only in terms of isolated dislocation motion but also in terms of interactions between dislocations in the whole network.

At higher frequencies (1 to 10^{-2} Hz) for internal friction measurements or at shorter loading time ($t < 100$ s) for microcreep experiments, dislocations are able to move in a reversible way under the applied stress. The restoring force is in that case induced by the line tension of dislocations pinned between quasi-immobile segments of the dislocation network (i.e. jogs, triple nodes, dislocations segments not in the basal plane...). The result is only anelasticity and distribution of the restoring forces becomes more regular when the dislocation density increases.

At lower frequencies (below 10^{-2} Hz) for internal friction measurements or for microcreep experiments with long-time loading ($t > 10^2$ s) the reversible motion of dislocation segments is accompanied by irreversible motion of « pinning points » on dislocations in the basal plane.

Thus, we have developed a model where the interactions of the whole network of dislocations is taken into account.

Let us consider a single crystal where a real network of dislocations can be found. When stress is applied, three features are obtained with the increasing stress :

i) dislocation segments take a certain curvature;
ii) dislocation nodes begin to move;
iii) dislocation density is increased.

Internal friction experiments done at 1 Hz are only dealing with i). When microdeformation occurs i.e. during microcreep or very low frequency experiments, all the features can be obtained. In our experiments, where special care is taken to keep microstructure constant, only i) and ii) are expected.

Our assumptions concerning the model are the following. Let us consider a single-crystal with a dislocation network corresponding to N mobile dislocation segments of length l (distributed or not). These segments are pinned at their ends by less mobile entities (nodes, jogs or super-jogs...). These dislocations are able to glide on the basal planes (for

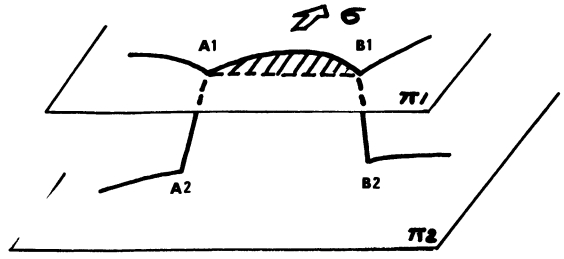

Fig. 6. — Schematic drawings of our model (π_1, π_2 are basal planes).

example π_1, and π_2 in figure 6). When an external stress τ is applied in these planes :

i) dislocation segment A_1B_1 will glide on π_1 according to the non-crystalline core model and will take a certain curvature;

ii) dislocation segments A_1A_2 and B_1B_2 will climb in non-basal planes under the effect of forces existing on A_1, A_2, B_1, B_2.

So, we can consider that gliding on π_1 is reversible when stress vanishes under the effect of line tension (anelasticity) and that climb motion on A_1A_2 and B_1B_2 is a non-reversible motion (viscoplasticity) if we neglect the variation of free enthalpy of the crystal.

Let us develop now each element of the motion :

4.1 GLIDE ON BASAL PLANE (π_1). — At point A_1 when stress is applied, the line tension T is in equilibrium with the resulting applied force F_{A_1} on dislocation segment A_1B_1 (Fig. 7) and

$$T = F_{A_1} = 1/2\, Gb^2$$

where G is the shear modulus, b the Burgers vector that is to say : $T\dfrac{\partial^2 y}{\partial x^2} = \tau . b$ then $y = \tau b/2\, T\,(l - x)\, x$ if $\overline{A_1B_1} = l$. The mean values

$$\bar{y} = \frac{1}{L}\int_0^l y\, dx = \sigma b L^2/12\, T .$$

The angle α is given by : $\tan \alpha = \sigma b\, l/2\, T$.

Over a maximum value of σ, σ_{max}, the segment A_1B_1 will curve up to an unstable position ($x = l/2$; $y = l/2$) giving possibilities to dislocation multiplication (by Franck and Read source for example) and :

$$\frac{\tau_{max}\, b}{2\, T} \times \frac{l}{2} = 1$$

so,

$$\tau_{max} = 4\, T/bl = 2\, Gb/l$$

τ_{max} will be the limit to the applied stress in our model (assumption of constant microstructure).

In regard with time, the variation of the curvature of dislocation segment A_1B_1 under stress τ, can be written as :

$$B\dot{U}_1 + KU_1 = \tau b \qquad (1)$$

where U_1 is the mean displacement of the segment, B the damping constant i.e. the inverse of the mobility F/v_d where F is the applied force on dislocation and v_d the dislocation velocity. For a « free » defect $B = \sigma b/v_d$ and in the model, v_d will be the dislocation velocity deduced from the non-crystalline core model [7].

K is the spring constant due to the line tension [19].

$$K = \tau \frac{Gb^2}{l^2} .$$

4.2 CLIMB MOTION OF A_1A_2. — First, it is necessary to know the force F_c acting on A_1 and A_2. A simple calculation gives [20] :

$$F_c = \frac{\frac{1}{2} Gb^2}{h} \cdot 2 \cos \beta$$

with h the distance between two planes π_1 and π_2.

We have $\cos \beta = \sin \alpha$ (Fig. 8) and for small angles

$$\sin \alpha \simeq \alpha \simeq \tan \alpha = \tau l/Gb$$

and $F_c = \tau bl/h$ by unit length.

Under the action of the force F_c on dislocation A_1A_2, this segment will climb thanks to jog diffusion. Let us consider one jog over each segment, which is a reasonable value according to concentration estimation [20]. Jog diffusion can be envisaged either in steady-state regime or with thermal activation.

4.2.1 *Diffusion in steady-state regime.* — Every time a vacancy is created (volume = b^3), it corresponds to

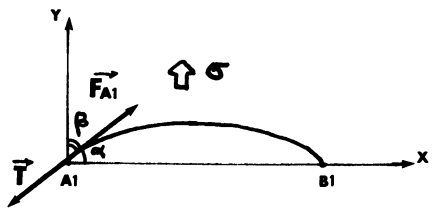

Fig. 7. — Glide movement of basal segment of dislocation A_1B_1 ($XA_1\ Y$ is in a basal plane).

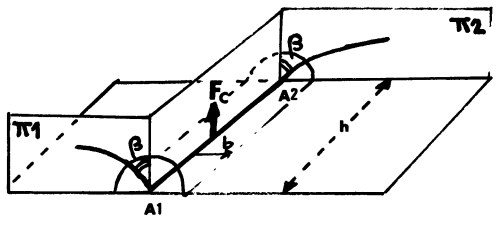

Fig. 8. — Climb movement of non-basal segment of dislocation A_1A_2 (π_1, π_2 are basal planes).

a mean displacement of dislocation (Fig. 8) :

$$\delta x = b^3/b.h = b^2/h .$$

As a consequence of force F_c acting on A_1A_2, the vacancy concentration near the dislocation (cylinder radius = b) will be equal to c and for every atomic position, the free energy will be expressed [21] by :

$$dF = kT \ln(c/c_0) - (\tau b^3\ l/h)$$

where c_0 is the vacancy concentration in the unstressed crystal. At equilibrium $dF = 0$ and

$$c = c_0 \exp \tau b^3\ l/h$$

with

$$c_0 = 1/b^3 \exp(-E_{fv}/kT)$$

the problem is then equivalent to a cylinder of radius b along A_1A_2 axis with vacancy concentration c inside and c_0 outside. Thus the motion of A_1A_2 will be governed by vacancy diffusion at the velocity :

$$\dot{U}_2 = \frac{\delta x}{\delta t}.$$

According to Fick's law

$$\frac{1}{S} \cdot \frac{1}{\delta t} = - D_v\left(\frac{c - c_0}{b}\right)$$

with D_v vacancy diffusion coefficient and $\dot{U}_2$ can be written :

$$\dot{U}_2 = \frac{b^2}{h} \cdot 4\pi b^2 \cdot \frac{D_v}{b} \cdot c_0\left[\exp \frac{\tau b^3\ l}{hkT} - 1\right]$$

or

$$\dot{U}_2 = \frac{4\pi D_{SD}}{h} \cdot \left[\exp \frac{\tau b^3\ l}{hkT} - 1\right] \qquad (2)$$

with D_{SD}, self-diffusion coefficient.

As the climb is governed by self-diffusion, another way to get the velocity is to apply Einstein's formula to the jog

$$\dot{U}'_2 = D_j\ F_c/kT$$

where D_j is the jog diffusion coefficient as

$$D_j = 4\pi b/h.D_{SD}$$

and

$$\dot{U}'_2 = 4\pi D_{SD}\ \tau b^3\ l/h^2\ kT\ . \qquad (3)$$

This result is the same as (2) in the weak stress approximation.

4.2.2 *Diffusion by thermal activation.* — In order to move A_1A_2 it is necessary to create a vacancy near the jog and make it migrate; the thermal activation is favoured by the force on A_1A_2. If ν is the frequency of these events which lead to a displacement of A_1A_2 equal to $a = b.b/h$ that is to say a work.

$$F_c.h.a = \tau b^3\ l/h$$

we get

$$\nu = \nu_0\left[\exp - \frac{E_{FV} + E_{MV} - \tau b^3\ l/h}{kT} - \exp - \frac{E_{FV} + E_{MV} + \tau b^3\ l/h}{kT}\right]$$

and

$$\dot{U}_2 = \nu \cdot a = 2\frac{D_{SD}}{h} \cdot \sinh \tau b^3\ l/hkT \qquad (4)$$

this result is not very different from (2) and (3). This relation will be used in the following part. In fact equation (4) corresponds only to the case where A_1B_1 is in equilibrium (i.e. $\dot{U}_1 = 0$ in (1)); when this is not the case ($U_1 < U_2$ equilibrium) it is necessary to change τb by KU_1 : in effect, the instantaneous position U_1 corresponds to an equilibrium resulting from the application of the fictive stress $\tau_{fict.}$ as

$$KU_1 = \tau_{fict.}.b .$$

We have to write in (4)

$$\dot{U}_2 = 2\frac{D_{SD}}{h} \sinh KU_1\ b^2\ l/hkT\ . \qquad (5)$$

4.3 Global motion of dislocation network. — According to figure 9 the whole displacement of dislocation A_1B_1 can be found by solving equations (1) and (5) with U_1 replaced by $(U_1 - U_2)$.

So we get

$$\dot{U}_1 = \frac{\tau b - K(U_1 - U_2)}{B} \qquad (6)$$

$$\dot{U}_2 = \frac{2\ D_{SD}}{h} \sinh \frac{K(U_1 - U_2)\ b^2\ l/h}{kT} \qquad (7)$$

and the deformation due to the dislocation motion will be taken as

$$\varepsilon_{disl.} = \rho.b.U_1 .$$

4.4 Numerical applications. — In order to compare this model to our experimental results a program has been developed. This program is able to simulate either microcreep experiment or internal friction measurement.

The applied stress (or maximum stress) can vary from 5×10^4 to 10^6 N m^2. The self-diffusion coefficient

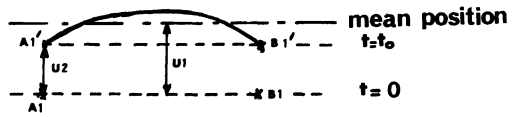

Fig. 9. — Global movement of dislocation segment A_1B_1.

has been taken as

$$D_{SD} = 1.5 \times 10^{-3} \exp(-0.62/kT)\ \mathrm{m}^2.\mathrm{s}^{-1}$$

according to Ramseier [22].

The program takes into account a distribution over the length of dislocations lying in the basal plane. To simplify our calculations the distribution is taken as uniform distribution.

$$N(l)\,\mathrm{d}l = C\,\mathrm{d}l$$

with

$$\rho = \int_0^{l_0} lC\,\mathrm{d}l$$

and

$$10^{-5} < l_0 < 2 \times 10^{-4}\,\mathrm{m}.$$

If we consider the displacement of dislocation segments which is not in the basal plane (A_1A_2), the velocity $\dot{U}_2$ will give nonlinear effects when

$$K(U_1 - U_2)\, b^2\, l/hkT \geqslant 1$$

or

$$\tau b^3\, l/hkT \simeq 10^{-4} \frac{l}{h} \geqslant 1.$$

In our conditions ($T \simeq 260$ K)

$$h \leqslant 10^{-4}\, l \simeq 10^{-8}\,\mathrm{m}.$$

So we will take

$$10^{-8} < h < 5 \times 10^{-8}\,\mathrm{m}$$

and under these conditions, $\dot{U}_2 \simeq 5 \times 10^{-7}$ m s^{-1} which is comparable to v_d and the dependence of $\tan\varphi$ when σ increases will be taken into account.

The limits of the model are obtained when Franck and Read sources are activated, that is to say when dislocation density increases.

For creep experiments, we obtain a maximum stress $\tau_{max} = 2\,Gb/l \simeq 3 \times 10^4\ \mathrm{N.m^{-2}}$ and when the loading time will be :

$$t_{max} = U_1/v_d \simeq 500\ \mathrm{s} \quad \text{at} \quad 250\ \mathrm{K}.$$

So for internal friction measurements the limit of the model will be attained when frequency decreases over 10^{-3} Hz.

4.4.1 *Microcreep measurement.* — We have made simulation for a loading time equal to 20 s and unloading. Simulations with different sets of parameters (l_0, ρ, h) were performed [23]. For dislocation density $\rho = 3 \times 10^9\ \mathrm{m}^2$, l_0 value equal to 10^{-4} m and $h = 2 \times 10^{-8}$ m strain rate were determined at 20 s for different stresses. On figure 10, we have plotted $\dot{\varepsilon}$ *versus* stress. We obtained results which are to be compared with our experimental results (for example Fig. 2b). A nonlinear effect is exhibited as the temperature gets higher than 250 K.

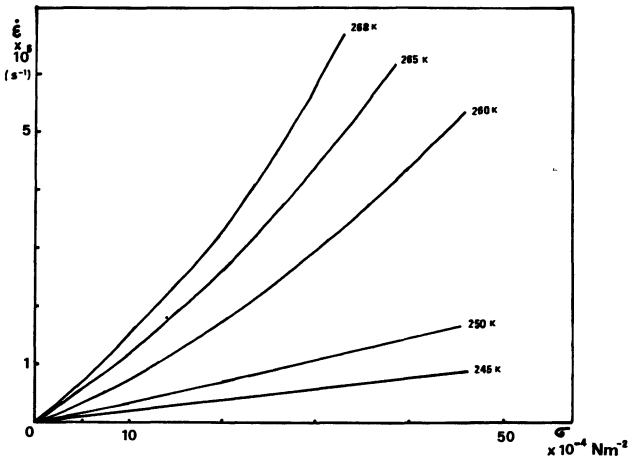

Fig. 10. — Simulated strain-rate *versus* stress curve. ($\rho = 3 \times 10^{-9}\ \mathrm{m}^{-2}$, $l_0 = 10^{-4}$ m, $h = 2 \times 10^{-8}$ m.). Strain-rate is taken after 20 s as in our experiments.

4.4.2 *Internal friction.* — In our program we calculate the deformation resulting from a sinusoidal stress $\sigma = \sigma_0 \sin \omega t$, that is to say, that calculation is made by an incremental method. Then internal friction is obtained from the area of the cycle, σ *versus* ε. The values are taken after one cycle in order to obtain a steady state deformation.

Our simulation gives curves as shown in figure 11.

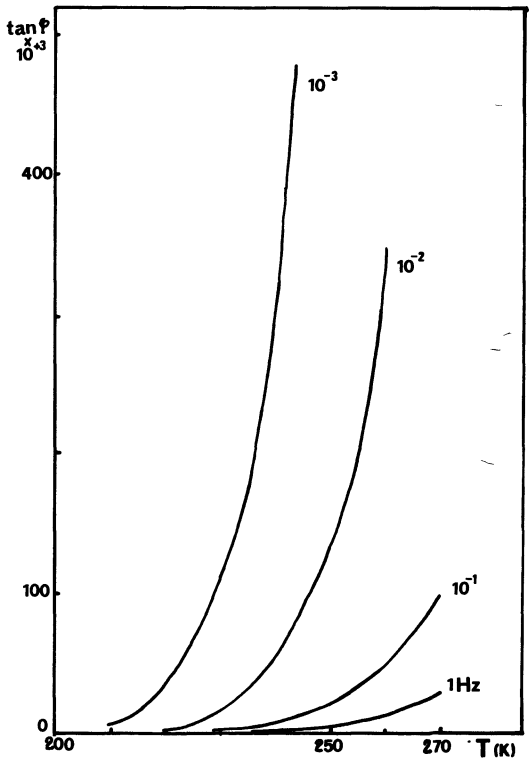

Fig. 11. — Internal friction *versus* temperature obtained from the model ($\rho = 3 \times 10^{-9}\ \mathrm{m}^{-2}$, $l_0 = 10^{-4}$ m, $h = 2 \times 10^{-8}$ m, $\sigma_0 = 5 \times 10^4\ \mathrm{N\,m^{-2}}$). Pure deformed ice.

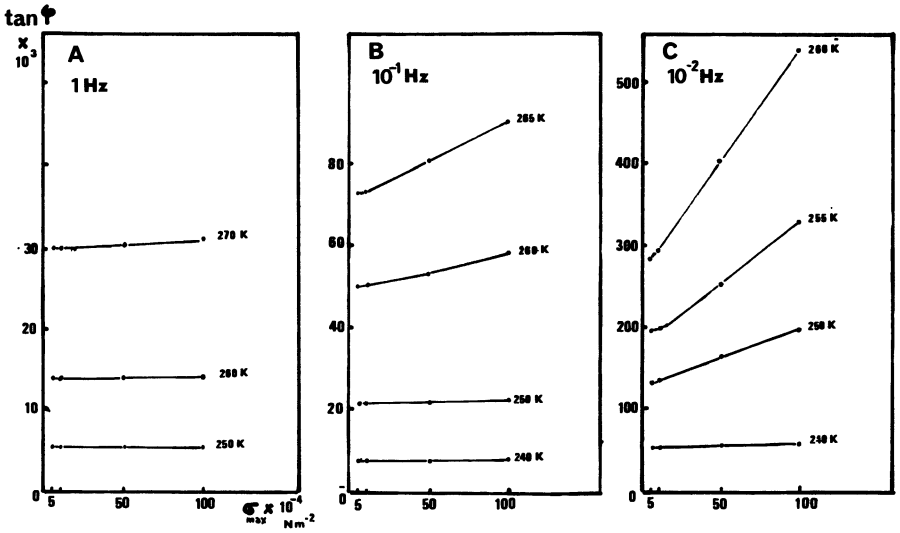

Fig. 12. — Theoretical internal friction *versus* maximum stress for different frequencies ($\rho = 3 \times 10^{-9}$ m^{-2}, $l_0 = 10^{-4}$ m, $h = 2 \times 10^{-8}$ m). Pure deformed ice

These theoretical results are very similar to our experimental results if we take $l_0 = 10^{-4}$ m, $h = 2 \times 10^{-8}$ m and density dislocations between 10^{+9} and 5×10^9 m^{-2}.

Values of the distribution parameter n have been calculated from these theoretical curves. We found $n = 0.72$ which is similar to the values found from our experimental values for deformed specimens of pure ice. Simulations were also done for HF-doped specimens [23] by introducing a higher dislocation velocity according to the non-crystalline core model [8].

Figure 12 exhibits our simulated results when σ_0 varies (i.e. the dependence on amplitude). Also in this case theoretical results are in agreement with experimental results shown in figure 4.

5. Conclusion.

The aim of our simulation was not to fit our experimental results exactly because too many parameters must be determined precisely (for example the distribution of dislocation segment lengths). But with reasonable values of parameters we are able to describe our experiments correctly.

To sum up internal friction measurements have been described at low frequency using a dislocation model assuming :

i) that dislocation density remains constant during experiments,

ii) the whole dislocation network is activated and

iii) the mechanism results from the interaction between dislocation glide on basal plane and dislocation climb in non-basal plane.

Of course, our simulation concerning this model has to be improved particularly by obtaining the value of physical parameters in order for it to fit better with our experimental data. Nevertheless, this model is able to take into account :

i) the dependence on frequency in internal friction measurements, according to a distribution of restoring forces;

ii) the dependence of internal friction on the amplitude of measurement.

Simulation of microcreep experiments (loading and unloading) gives reasonable values for strain-rate and recovery.

References

[1] GLEN, J. W., *Phys. Cond. Mat.* **7** (1968) 43-51.

[2] PEREZ, J., TATIBOUET, J., VASSOILLE, R., GOBIN, P. F., *Philos. Mag.* **31** n° 5 (1975) 985-999.

[3] WHITWORTH, R. W., PAREN, J. G., GLEN, J. W., *Philos. Mag.* **33** n° 3 (1976) 409-426.

[4] FROST, H. J., GOODMAN, D. J., ASHBY, M. F., *Philos. Mag.* **33** n° 6 (1976) 951-961.

[5] WHITWORTH, R. W., *Philos. Mag.* **41** n° 4 (1980) 521-528.

[6] MAI, C., *C. R. Hebd. Sean. Acad. Sci.* **282** n° 22 (1976) 515-518.

[7] PEREZ, J., MAI, C., VASSOILLE, R., *J. Glaciol.* **21** n° 85 (1978) 361-374.

[8] PEREZ, J., MAI, C., TATIBOUET, J., VASSOILLE, R., *J. Glaciol.* **23** n° 91 (1980) 133-149.

[9] VASSOILLE, R., MAI, C., PEREZ, J., *J. Glaciol.* **21** n° 85 (1978) 375-384.

[10] TATIBOUET, J., PEREZ, J., VASSOILLE, R., *J. Phys. Chem.* **87** n° 21 (1983) 4050-4054.

[11] ETIENNE, S., CAVAILLE, J. Y., PEREZ, J., SALVIA, M., *J. Physique Colloq.* **42** (1981) C5-1129-C5-1134.

[12] LAZAN, B. J., *Structural Damping* (Oxford-Pergamon Press) p. 1-34.

[13] PEREZ, J., PEGUIN, P., GOBIN, P. F., *Brit. J. Appl. Phys.* **16** (1965) 1347-1351.

[14] TATIBOUET, J., PEREZ, J., VASSOILLE, R., *J. Physique Colloq.* **42** (1981) C5-541-546.

[15] BASS, R., *Z. Phys.* **153** (1958) 16-37.

[16] GOSAR, P., *Philos. Mag.* **29** (1974) 221-240.

[17] SCHOECK, G., BISOGNI, E., SHYNE, J., *Acta Metall.* **12** (1964) 1466-1468.

[18] JOHARI, G. P., JONES, S. J., *J. Chem. Phys.*, to be published.

[19] BENOIT, W., GREMAUD, G., SCHALLER, R., *Plastic deformation of amorphous and semi-crystalline materials,* Les Houches (Editions de Physique) 1982, p. 65-91.

[20] FRIEDEL, J., *Dislocations, Solid State Physics* **3** (Pergamon Press, New York) 1964, p. 105-111.

[21] HIRTH, J. P., LOTHE, J., *Theory of Dislocations* (McGraw Hill, New York) 1968, p. 506-513.

[22] RAMSEIER, R. O., *J. Appl. Phys.* **38** (1967) 2553-2556.

[23] TATIBOUET, J., PEREZ, J., VASSOILLE, R., International Conference on Internal Friction and Ultrasonic Attenuation in Solids, June 1985, Urbana, USA.